Journal of Materials Chemistry A

Accepted Manuscript

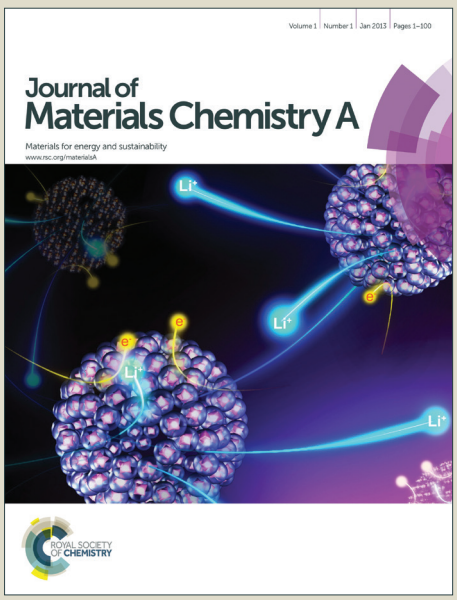

ROYAL SOCIETY OF CHEMISTRY

www.rsc.org/materialsA

Dendrite growth in the recharging process of zinc-air battery

Keliang Wang, Pucheng Pei *, Ze Ma, Huicui Chen, Huachi Xu, Dongfang Chen and Xizhong Wang

State Key Lab. of Automotive Safety and Energy, Tsinghua University, Beijing 100084, China

Abstract

To improve cycling performance of rechargeable zinc-air batteries, dendritic morphology of electrodeposited zinc should be effectively controlled. It is of crucial importance to understand the formation mechanism of zinc dendritic structure. Here we show that a phase-field model of electrochemistry is established to simulate dendrite growth of electrodeposited zinc, and several measures including the pulsating current and the electrolyte flow are taken to suppress dendrite growth in the charging process. The results demonstrate that dendrite propagation is mainly controlled by diffusion dependent upon overpotential and surface energy anisotropy, and dendritic morphology can also give rise to non-uniform distribution of electric field and ion concentration in the electrolyte. The proposed model and solutions will be available for studying dendrite growth of metal-air batteries as well as metal

* Corresponding author. Tel. /fax: +86-10-62788558.
E-mail address: pchpei@mail.tsinghua.edu.cn (p.pei).

electrodeposition.

Keywords: Dendrite growth; Phase-field model; Mechanism; Solutions

1. Introduction

Recently, zinc-air batteries have received more attention mainly because of their higher energy density,[1-4] which can be applied to a variety of fields including stationary energy storage,[5, 6] consumer electronics,[7] transport,[8] and defense.[9] However, lifetime problem of rechargeable zinc-air batteries limits its commercial application.[10, 11] Dendrite growth is one of key factors influencing cycle life of the battery, which has always been the research focus.[12, 13]

Although dendrite growth of electrodeposited zinc has been widely studied for nearly 50 years, the mechanism of dendrite growth has yet to be understood. To study dendrite formation of electrochemistry, a few numerical models were developed. Matsushita et al. utilized the diffusion-limited aggregation model to simulate zinc electrodeposition process from the perspective of one dimension.[14, 15] Guyer et al. addressed a thin-interface phase-field model for electrochemical process to study the effect of the applied voltage on the morphological transition.[16-19] Chen et al. proposed a nonlinear phase field model for electrodeposition.[20-23] To facilitate observation on growth behavior of dendrites and morphological characteristics in the process of electrodeposition, some kinds of instruments can be employed such as scanning electron microscopy,[24-26] transmission electron microscopy,[27] optical

microscopy,[28] and atomic force microscopy.[29] Some researchers have already conducted investigations on the mechanism of zinc dendrite growth. Diggle et al.[30] proposed that dendrite growth of electrodeposited zinc would be controlled by activation, while Wang[31] stated that dendrite growth was controlled by diffusion. Other researchers are committed to studying morphological control of electrodeposited zinc by means of charging modes and electrolyte management. Shaigan et al.[32] employed pulsating currents to suppress the dendrite growth of electrodeposited zinc. Naybour[33] studied the effect of electrolyte flow on morphologies of electrodeposited zinc. Wang et al.[34] studied morphological control of zinc regeneration in the recharging process. Banik et al.[35] reported the use of branched polyethylenimine as an effective electrolyte additive for suppressing dendrite growth during electrodeposition.

In this work, a phase-field model for dendrite growth of electrodeposited zinc was established by means of COMSOL software, and effective solutions were also proposed to inhibit dendrite growth on the basis of the model. Meanwhile the mechanism of dendrite growth was further investigated based on the numerical simulation and experimental analysis.

2. Methodology

2.1. Numerical model

To deeply delve into dendritic growth of electrodeposited zinc, we

established a phase-field model of electrochemical reaction in COMSOL Multiphysics 4.3 based on Ginzburg-Landau free energy function. Here the phase-field model is under the assumption of the solid-liquid interface evolution proportional to interface free energy combined with electric energy. A series of governing equations including the phase-field equation (1), the ion diffusion equation (2), and the conservation of charge equation (3) can be expressed as follows:

$$\frac{\partial \xi}{\partial t} = L_\sigma \left[-\frac{\partial}{\partial x}\left(\kappa\kappa' \frac{\partial \xi}{\partial y} \right) + \frac{\partial}{\partial y}\left(\kappa\kappa' \frac{\partial \xi}{\partial x} \right) + \nabla\cdot(\kappa^2 \nabla \xi) + \frac{\partial g(\xi)}{\partial \xi} + \frac{\partial h(\xi)}{\partial \xi} \xi(1-\xi)(\xi - 0.5 + \eta) \right] \quad (1)$$

where ξ is the order parameter for distinguishing the electrode $(\xi = 1)$ and the electrolyte $(\xi = 0)$, L_σ is the interface mobility, η is the activation overpotential. $\kappa = \bar{\kappa}\left(1 + \delta \cos(\lambda\theta)\right)$ is anisotropy surface energy for the depositing morphology, where $\bar{\kappa}$ is a constant, θ is the angle between the normal vector of interface and a certain direction, δ is the strength of surface energy anisotropy and λ is a mode number of the anisotropy. $g(\xi) = W\xi^2(1-\xi)^2$ is a double-well free energy function describing the two equilibrium states for the electrode and the electrolyte in case of no electric field. $h(\xi) = \xi^3(10 - 15\xi + 6\xi^2)$ is an interpolating function for the electrode-electrolyte interface.

$$\frac{\partial C_{Zn^{2+}}}{\partial t} = \nabla\cdot\left(D_{Zn^{2+}}(\xi) \nabla C_{Zn^{2+}} \right) - C_{Zn^{2+}} \frac{\partial \xi}{\partial t} \quad (2)$$

where $D_{Zn^{2+}}(\xi) = (D^S_{Zn^{2+}} - D^L_{Zn^{2+}})h(\xi) + D^L_{Zn^{2+}}$ is the diffusivity of zinc ion, $D^L_{Zn^{2+}}$ is

the diffusivity of zinc ion at the electrode surface, $D^{L}_{Zn^{2+}}$ is the diffusivity of zinc ion in the electrolyte, $C_{Zn^{2+}}$ is the concentration of zinc ion in the electrolyte.

$$\frac{\partial \phi}{\partial t} = \gamma \frac{\partial \xi}{\partial t} - \nabla\cdot\left(\sigma(\xi)\nabla\phi\right) \tag{3}$$

where $\sigma(\xi)=(\sigma^{S}-\sigma^{L})h(\xi)+\sigma^{L}$ is the conductivity, σ^{S} is the conductivity of the electrode, σ^{S} is the conductivity of the electrolyte, ϕ is the potential in the electrolyte, and γ is the constant.

The boundary conditions were assumed in the phase-field model, where zinc ion concentration is applied at the electrolyte side in equation (2), and electric potentials are constant at both sides of the electrode and the electrolyte in equation (3).

Ions transport in the electrolyte is mainly caused by migration, diffusion, and convection, where migration is dependent upon electric field, diffusion upon ion concentration gradient, and convection upon electrolyte hydrodynamics. The material balance equation can be written by:

$$v\cdot\nabla C_{Zn^{2+}} - \nabla\cdot\left(D_{Zn^{2+}}\nabla C_{Zn^{2+}} + z\mu_{Zn^{2+}}FC_{Zn^{2+}}\nabla\phi_{l}\right) = R_{Zn^{2+}} \tag{4}$$

where z is the valence of zinc, $\mu_{Zn^{2+}}$ is the mobility of the charged species, F is Faraday's constant, ϕ_{l} is electrolyte potential, and $R_{Zn^{2+}}$ is zinc ion reaction rate.

The model of electrolyte movement employs Navier-Stokes equation, assuming that the electrolyte flow is incompressible and Newtonian.

$$\rho\left(v\nabla v\right)=-\nabla p+\mu\nabla^2 v+f \quad (5)$$

where ρ is the electrolyte density, μ is dynamic viscosity, and f is the driving force.

2.2. Experimental

To further study the mechanism of dendrite growth, a set of experiments of electrodeposited zinc was carried out under different conditions of current densities, flowing velocities. In addition, the morphologies of electrodeposited zinc were examined by scanning electron microscopy (TS5136XM, JSM-6460).

The cycling performance of rechargeable zinc-air battery in a tri-electrode configuration was tested, where a nickel mesh was employed as the third electrode, stainless steel as zinc electrode, three layers structure as the air electrode, and a 7M potassium hydroxide mixed with 0.6M zinc oxide as the electrolyte. The effective area of electrodes was about 900 mm^2, and the distance between the anode and the cathode was 5 mm. The experiment on the internal resistance of the battery was conducted by means of a CHI660D electrochemical workstation. The impedance spectra were recorded by sweeping frequencies over the range of 20000 Hz-0.1 Hz with the amplitude of 0.05 V.

3. Results and discussion

3.1. Formation mechanism of zinc dendrite

Dendrite growth evolution can be simulated by means of the phase-field model, as illustrated in Fig. 1, where a plurality of nuclei at the bottom edge gradually grows into dendrites perpendicular to the cathode surface. The bonding energy of zinc atom in a certain direction is stronger than that in other directions, leading to dendrite formation[31]. As time goes on, the tip of protrusion starts to split, and branches grow symmetrically on the main stem. More importantly, dendritic morphology is agreed with experimental observation at upper right corner, namely dendrite structure consists of a backbone parallel to the electric field direction and many a branches adherent to both sides of the backbone at a certain angle.

Several studies have shown that dendritic morphology of electrodeposited zinc would occur when the overpotential reaches a certain value.[30, 31] Dendrite growth depends on local overpotential which is related to electric potential in the electrolyte, so dendrite can grow faster when the larger voltage is applied between the anode and the cathode. Fig. 2 (a) demonstrates that the overpotential would be larger at the high voltages, and dendrite grows more quickly. This also means that the higher the overpotential is, the shorter initiation time of dendrite growth becomes. Fig. 2 (b) shows the effect of interface energy anisotropy on dendritic morphology based on the phase-field model, where dendrites grow higher at the large strength of surface energy anisotropy δ.

The equilibrium system of the electrode-electrolyte interface is broken down

due to electrochemical reaction ($Zn^{2+} + 2e^- \rightarrow Zn$). Fig. 3 (a) shows the evolution of phase variables including the electric potential ϕ , zinc ion concentration $C_{Zn^{2+}}$ and the phase parameter ξ across the interface during electrodeposition, where the electric potential is able to decrease because of activation impedance and ohmic resistance, and concentration gradient of zinc ion will be formed on account of electrochemical reaction and ion diffusion as the phase parameter varies from the liquid phase to the solid phase. Fig. 3 (b-d) demonstrates the effect of electrodepositing morphology on the electric field and zinc ion concentration based on the phase-field simulation. It can be found that zinc ion concentration and electric potential at the tip of deposits are higher than those at other positions, leading to concentration gradient and heterogeneity of local current densities in the neighborhood of epitaxial morphology. Additionally, non-uniformity of the electric potential and ion concentration can also promote dendrite growth.

3.2. Influence factors of dendrite growth

Dendritic morphology gives rise to ion concentration gradient and non-uniform distribution of electric potential according to the phase-field model. As a result, it is necessary to increase electrolyte hydrodynamics and change the charging mode for suppressing dendrite growth.

Fig. 4 shows zinc ion concentration distribution and the local current density for different Reynolds numbers. The higher flow velocity for the higher Reynolds number can not only reduce zinc ion concentration gradient, but

might also increase the local current density significantly due to the increased transport velocity of zinc ions. This will cause much more ions to participate in the electrochemical reaction and the depositing morphology more uniformly. In addition, the electrolyte flow can also increase ions diffusion, resulting in reduction of the electrolyte resistance. Fig. 5 displays total ohmic resistances of zinc-air battery during charging, where ohmic resistance in the electrolyte reduces with the increase of Reynolds number.

Fig. 6 shows that different morphologies of electrodeposited zinc can be obtained at different charging current densities, where leaf-like morphology would be easily formed at the high current density of 100 mA cm^{-2} in Fig. 6 (a), demonstrating that dendrites symmetrically grow on both sides of main stems. Such fractal growth may be stemmed from powerful surface energy anisotropy, leading to limited diffusion of atoms. It is well-known that electrochemical reaction rate will reduce with the decrease of current density, and the effect of electric field force on depositing atoms becomes weak, thereby these atoms have much more possibility to transfer. It can be found in Fig. 6(b)-(d) that dendritic morphology does not happen at low current densities, and activation energy need to be overcome by the depositing atoms.

The depositing morphology behaves like uniform and compact at low current densities. However, the dendritic morphology of electrodeposited zinc is more evenly but uncompacted at large current densities, as shown in Fig. 7 (a). To solve the problem of dendrite growth in the case of fast charge, several

solutions like electrolyte management and charging modes were employed, namely electrolyte flow and pulsating current. It can be seen from Fig. 7 (b) that orientation of dendrite growth is not perpendicular to the electrode surface. The orientation change may be caused by the flowing electrolyte shifting the electrodeposited atoms of low energy. If the flowing velocity is too high, a large amount of deposited zinc might be scraped off the cathode surface, thus decreasing the charging efficiency. Fig. 7 (c) illustrates the boulder-like morphology of deposited zinc under the condition of pulsating current of 20% duty cycle. Atoms have much more time to diffuse under the condition of the pulsating current, meaning that dendritic morphology is controlled by diffusion. In addition, zinc ions in the electrolyte can obtain more energy at high temperature, which can overcome the obstacles of electric field force and electrochemical reaction of concentration gradient, thus retarding dendrite growth to some extent (Fig. 7(d)).

It can be found that dendrite growth of electrodeposited zinc is controlled by diffusion in accordance with the above mentioned. Furthermore, exterior electrolyte environment can only suppress but not eradicate dendritic growth, while charging modes could fundamentally change the morphology of deposited zinc. Besides, the electrolyte flow can shape the orientation of dendrite growth, and pulsating currents or low current can change the morphology of electrodeposited zinc.

3.3. Cycling performance

Fig. 8(a) shows the charge-discharge polarization curve of rechargeable zinc-air battery in a tri-electrode configuration. Dendrites grow rapidly under the condition of fast charge, leading to the short circuit between the anode and the cathode, and thus reducing cycle life of rechargeable zinc-air battery. To highlight the effect of dendritic morphology on the cycling performance of rechargeable zinc-air battery, the large charging current density of 50 mA cm^{-2} was used in this experiment. Fig. 8(b) shows that the lifetime of the battery is very short for the lower Reynolds number, and discharging voltage sharply decrease due to morphological change. This implies that the flow velocity of the electrolyte plays a great role in retarding dendrite growth. In addition, the electrolyte flow can also carry off oxygen bubbles, keeping the voltage stable in the recharging process of the battery. The uniform morphology change of zinc electrode in the charge-discharge process is of great importance to the lifetime of zinc-air batteries, so it is necessary to inhibit dendrite growth. Moreover, the charging capacity is related to morphologies of electrodeposited zinc.

4. Conclusions

The mechanism of dendrite growth of electrodeposited zinc was investigated by means of phase-field simulation and electrodeposition experiment, and the related solutions to suppressing dendrite growth were also put forward, which can be conducive to studying on the cycle life of zinc-air batteries or other

metal-air batteries. The conclusions in detail are as follows:

1) The phase-field model for dendrite growth of electrodeposited zinc was developed, where the liquid-solid interface transformation can display dendritic morphology and dendrite growth evolution. In addition, the model can be used for analyzing the effect of dendrite growth on the electric potential and zinc ion concentration gradient in the electrolyte.

2) Solutions to dendrite growth were proposed including charging modes and electrolyte management, where low current can inhibit dendrite growth due to low activation overpotential, and pulsating current and electrolyte flow can retard dendrite growth or shape the direction of dendrite growth because of zinc ion diffusion enhancement in the electrolyte.

3) The morphology of electrodeposited zinc at the early stage is mainly dependent upon activation control, while dendrite growth at the late stage is stemmed from diffusion-limited control of zinc ions.

Acknowledgements

This work is supported by National Natural Science Foundation of China (21376138), National Basic Research Program of China (973 Program) (2012CB215505), and Tsinghua University Initiative Scientific Research Program

.

References

1 Y. Li and H. Dai, Recent advances in zinc-air batteries, *Chem. Soc. Rev.,* 2014, 43(15), 5257-5275.

2 P. Pei, Z. Ma, K. Wang, X. Wang, M. Song and H. Xu, High performance zinc air fuel cell stack, *J. Power Sources*, 2014, 249, 13-20.

3 M. Armand and J. Tarascon, Building better batteries, *Nature*, 2008, 451(7179), 652-657.

4 M. Prabu, P. Ramakrishnan, H. Nara, T. Momma, T. Osaka and S. Shanmugam, Zinc-air battery: understanding the structure and morphology changes of graphene-supported $CoMn_2O_4$ bifunctional catalysts under practical rechargeable conditions, *ACS Appl. Mater. Interfaces*, 2014, 6(19),16545-16555.

5 B. Dunn, H. Kamath and J. Tarascon, Electrical energy storage for the grid: A battery of choices, *Science*, 2011, 334(6058), 928-935.

6 J. Rugolo and M.J. Aziz, Electricity storage for intermittent renewable sources, *Energy Environ. Sci.*, 2012, 5(5), 7151-7160.

7 J. Goldstein, I. Brown and B. Koretz. New developments in the electric fuel zinc-air system, *Proceedings of the 21st International Power Sources Symposium*,1999.

8 J. F. Cooper, D. Fleming, D. Hargrove, R. Koopman and K. Peterman, A refuelable zinc/air battery for fleet electric vehicle propulsion, 1995, *SAE Technical Paper*.

9 J. P. Fanucci, N. Gravelle and S. A. Schoenholtz, Powered unmanned aerial vehicle, 2010, *Google Patents*.

10 K. Wang, P. Pei, Z. Ma, H. Chen, H. Xu, D. Chen and H.Xing, Growth of oxygen

276 bubbles during recharge process in zinc-air battery, *J. Power Sources*, 2015, 296, 40-45.
277 11 M. Prabu, P. Ramakrishnan and S. Shanmugam, $CoMn_2O_4$ nanoparticles anchored on
278 nitrogen-doped graphene nanosheets as bifunctional electrocatalyst for rechargeable
279 zinc-air battery, *Electrochem. Commun.*, 2014, 41, 59-63.
280 12 K. Harting, U. Kunz and T. Turek, Zinc-air batteries: prospects and challenges for
281 future improvement, *Z. Phys. Chemie-Int. J. Res. Phys. Chem. Chem. Phys.*, 2012,
282 226(2), 151-166.
283 13 P. Pei, K. Wang and Z. Ma, Technologies for extending zinc-air battery's cyclelife: A
284 review, *Appl. Energy*, 2014, 128, 315-324.
285 14 M. Matsushita, M. Sano, Y. Hayakawa, H. Honjo and Y. Sawada, Fractal structures of
286 zinc metal leaves grown by electrodeposition, *Phys. Rev. Lett.*, 1984, 53(3), 286.
287 15 C. P. Chen and J. Jorné, Fractal analysis of zinc electrodeposition, *J. Electrochem.*
288 *Soc.*, 1990, 137(7), 2047-2051.
289 16 J. E. Guyer, W. J. Boettinger, J. A. Warren, and G. B. McFadden, Phase field modeling
290 of electrochemistry I: Equilibrium, *Phys. Rev. E*, 2004, 69(1), 021603.
291 17 J. E. Guyer, W. J. Boettinger, J. A. Warren, and G. B. McFadden, Phase field modeling
292 of electrochemistry. II. Kinetics, *Phys. Rev. E*, 2004, 69(2), 021604.
293 18 Y. Shibuta, Y. Okajima and T. Suzuki, Phase-field modeling for electrodeposition
294 process, *Sci. Technol. Adv. Mater.*, 2007, 8(6), 511-518.
295 19 Y. Shibuta, Y. Okajima and T. Suzuki, A phase-field simulation of bridge formation
296 process in a nanometer-scale switch, *Scr. Mater.*, 2006, 55(12),1095-1098.
297 20 L. Liang, Y. Qi, F. Xue, S. Bhattacharya, S. J Harris, and L. Chen, Nonlinear

phase-field model for electrode-electrolyte interface evolution, *Phys. Rev. E*, 2012, 86(5), 051609.

21 L. Liang and L. Chen, Nonlinear phase field model for electrodeposition in electrochemical systems, *Appl. Phys. Lett.*, 2014, 105(26), 263903.

22 H. Zhang, Z. Liu, L. Liang, L. Chen, Y. Qi, S. J Harris, P. Lu and L. Chen, Understanding and predicting the lithium dendrite formation in li-ion batteries: Phase field model, ECS Transactions, 2014, 61(8), 1-9.

23 D. A. Cogswell, Toward quantitative phase-field modeling of dendritic electrodeposition, arXiv preprint arXiv:1411.6615, 2014.

24 C. W. Lee, K. Sathiyanarayanan, S. W. Eom, M. S. Yun, Novel alloys to improve the electrochemical behavior of zinc anodes for zinc/air battery, *J. power sources*, 2006. 160(2), 1436-1441.

25 L. Xu, Y. Guo, Q. Liao, J. Zhang and D. Xu, Morphological control of ZnO nanostructures by electrodeposition, *J. Phys. Chem. B,* 2005, 109(28),13519-13522.

26 J. F. Parker, C. N. Chervin, E. S. Nelson, D. R. Rolison and J. W. Long, Wiring zinc in three dimensions re-writes battery performance-dendrite-free cycling, *Energy Environ. Sci.*, 2014, 7, 1117.

27 E. R. White, S. B. Singer, V. Augustyn, W. A. Hubbard, M. Mecklenburg, B. Dunn and B. C. Regan, In situ transmission electron microscopy of lead dendrites and lead ions in aqueous solution, *ACS nano*, 2012, 6(7), 6308-6317.

28 F. Chen, F. Mao, Z. Xuan, G. Yan, J. Han, T. Wang, Z.Cao, Y. Fu and T. Xiao, Real time investigation of the grain refinement dynamics in zinc alloy by synchrotron

microradiography, *J. Alloy. Compd.*, 2015, 630, 60-67.

29 J. S. Keista, C. A. Orme, P. K. Wright and J. W. Evans, An in situ AFM Study of the evolution of surface roughness for zinc electrodeposition within an imidazolium based ionic liquid electrolyte, *Electrochim. Acta*, 2015, 152, 161-171.

30 J. W. Diggle, A. R. Despic and J. Bockris, The mechanism of the dendritic electrocrystallization of zinc, *J. Electrochem. Soc*., 1969, 116(11), 1503-1514.

31 R. Y. Wang, The morphology study of zinc electrodeposits from alkaline zincate solutions. Vol. 68. 2006.

32 N. Shaigan, W. Qu and T. Takeda, Morphology control of electrodeposited zinc from alkaline zincate solutions for rechargeable zinc air batteries, *ECS Transactions*, 2010, 28(32), 35-44.

33 R. D. Naybour, The effect of electrolyte flow on the morphology of zinc electrodeposited from aqueous alkaline solution containing zincate ions, *J. Electrochem. Soc.*, 1969, 116(4, 520-524.

34 K. Wang, P. Pei, Z. Ma, H. Xu, P. Li and X. Wang, Morphology control of Zinc regeneration for zinc-air fuel cell and battery, *J. Power Sources*, 2014, 271, 65-75.

35 S. J. Banik and R. Akolkar, Suppressing dendritic growth during alkaline zinc electrodeposition using polyethylenimine additive, *Electrochim. Acta*, 2014.

Fig. 1. Dendrite growth evolution of electrodeposited zinc by means of the phase-field simulation

Fig. 2. The mechanism for dendrite growth, (a) the relationship between dendrite growth and the applied voltage under the same electric quantity condition, (b) the effect of surface energy anisotropy on dendritic morphology of electrodeposited zinc

Fig. 3. The effects of depositing morphology, (a) a phase-field model of zinc electrodeposition, (b) the depositing morphology of the phase-field simulation, (c) zinc ion concentration distribution, (d) the electric potential distribution

Fig. 4. The effect of the flowing electrolyte with several Reynolds numbers on the distribution of zinc ion concentration and local current density

Fig. 5. Nyquist plot of rechargeable zinc-air battery at different Reynolds numbers during charging

Fig. 6. Morphologies of electrodeposited zinc under the conditions of different current densities in 7M KOH with 0.6 M zinc oxide, (a) 100 mA cm^{-2} for 10 min, (b) 50 mA cm^{-2} for 20 min, (c) 20 mA cm^{-2} for 50 min, (d) 10 mA cm^{-2} for 100 min

Fig. 7. Morphological control of zinc regeneration at the current density of 100 mA cm^{-2} for 10 min, (a) dendritic morphology of electrodeposited zinc in the static electrolyte, (b) the morphology of electrodeposited zinc in the flowing electrolyte (0.05 m s^{-1}), (c) boulder-like morphology of zinc at the pulsating current of 20% duty cycle in the static electrolyte, (d) the morphology of electrodeposited zinc at the high temperature (60 ℃).

Fig. 8. Performance of rechargeable zinc-air battery, (a) charge and discharge polarization curves of the battery, (b) cycling performance of the battery at different Reynolds numbers

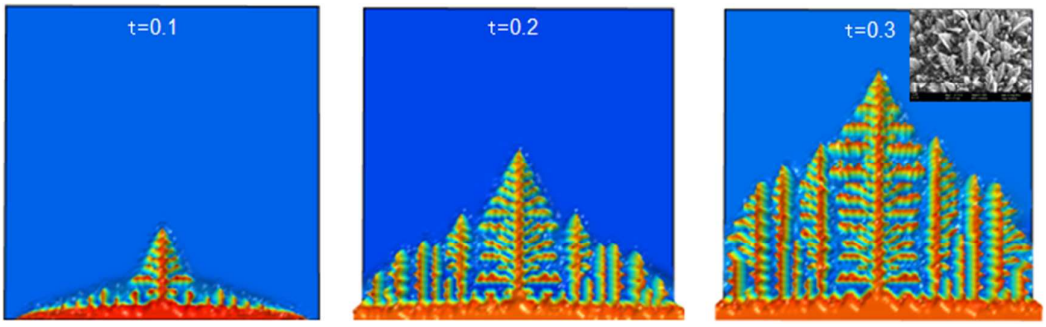

Fig. 1

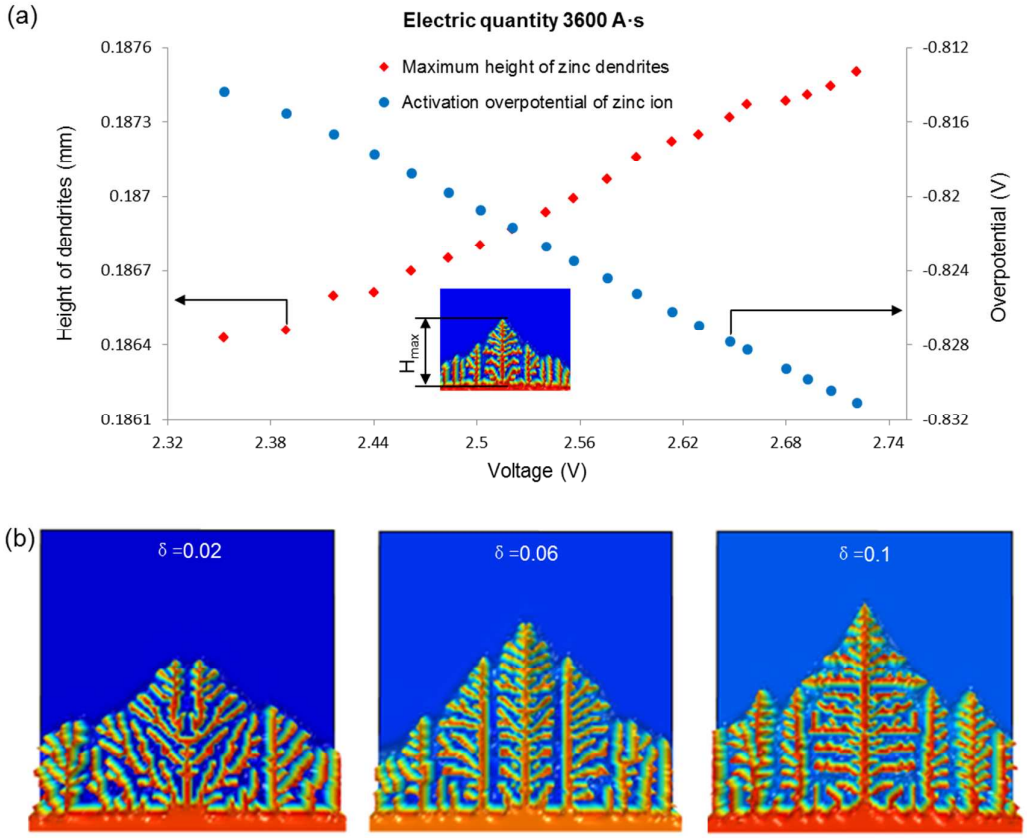

Fig. 2

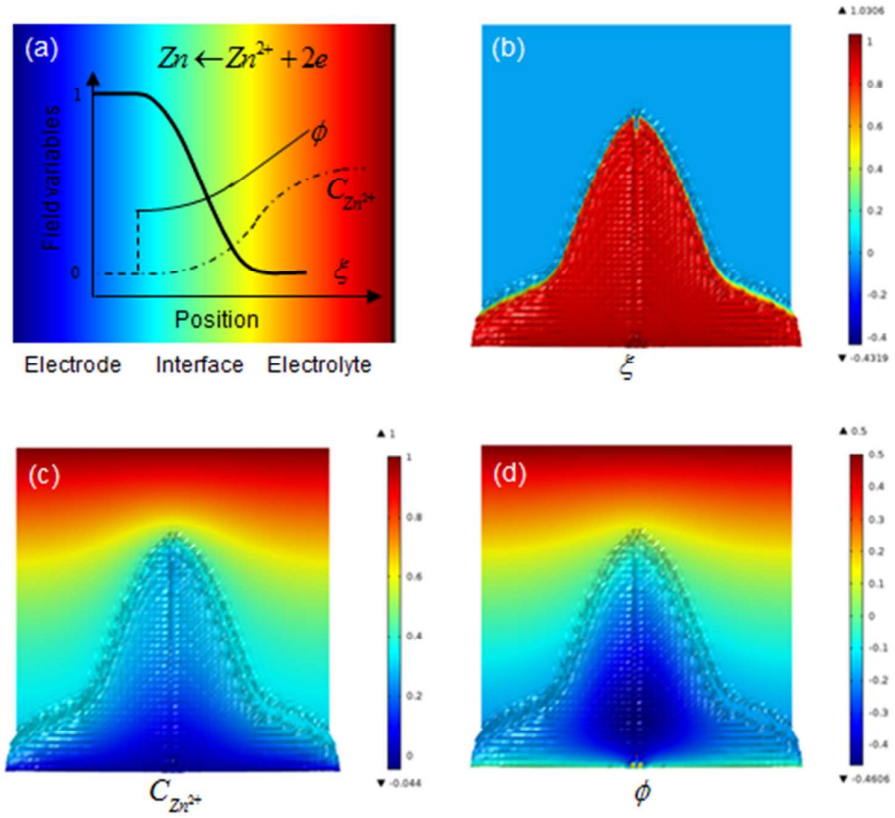

Fig. 3

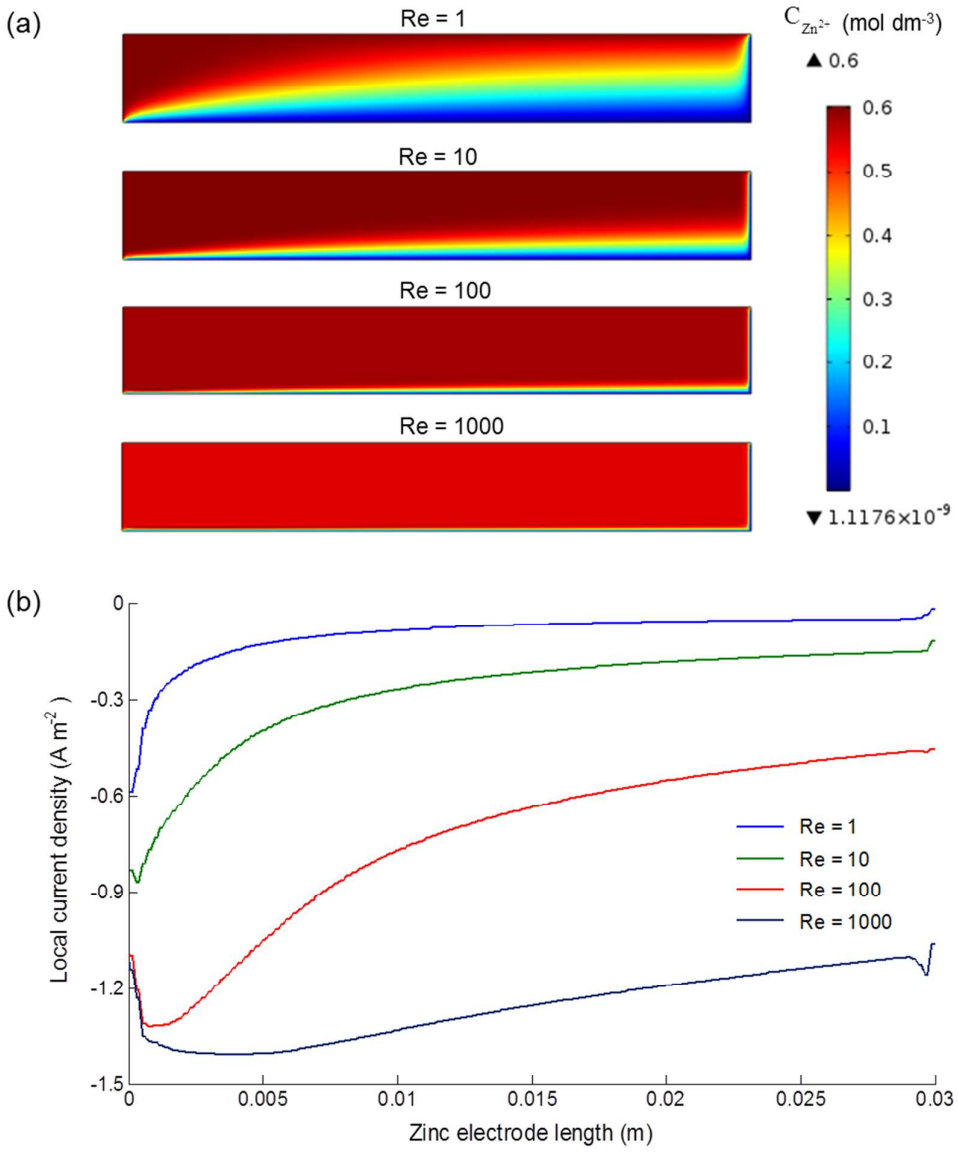

Fig. 4

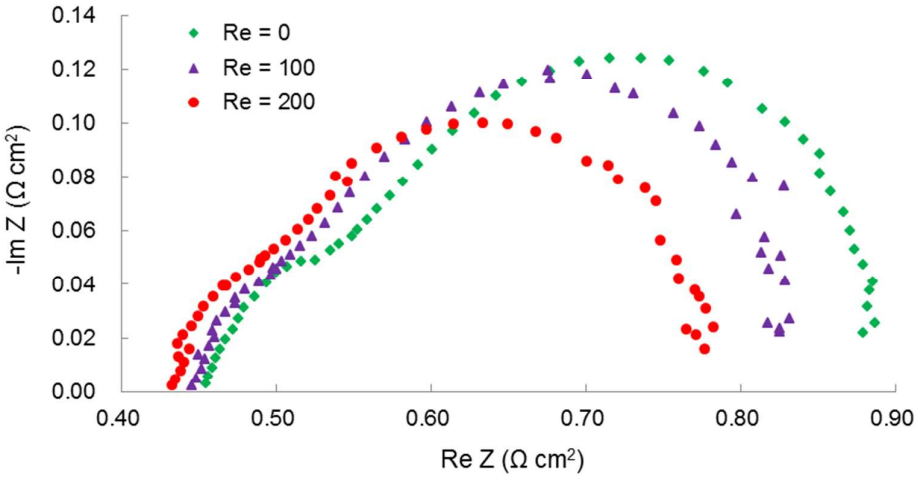

Fig. 5

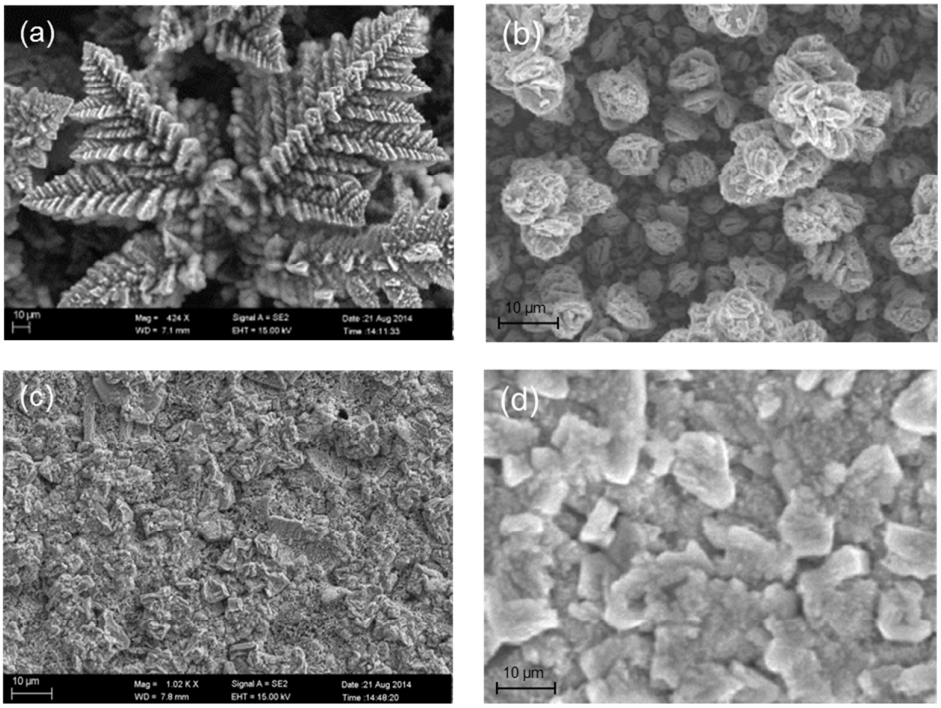

Fig. 6

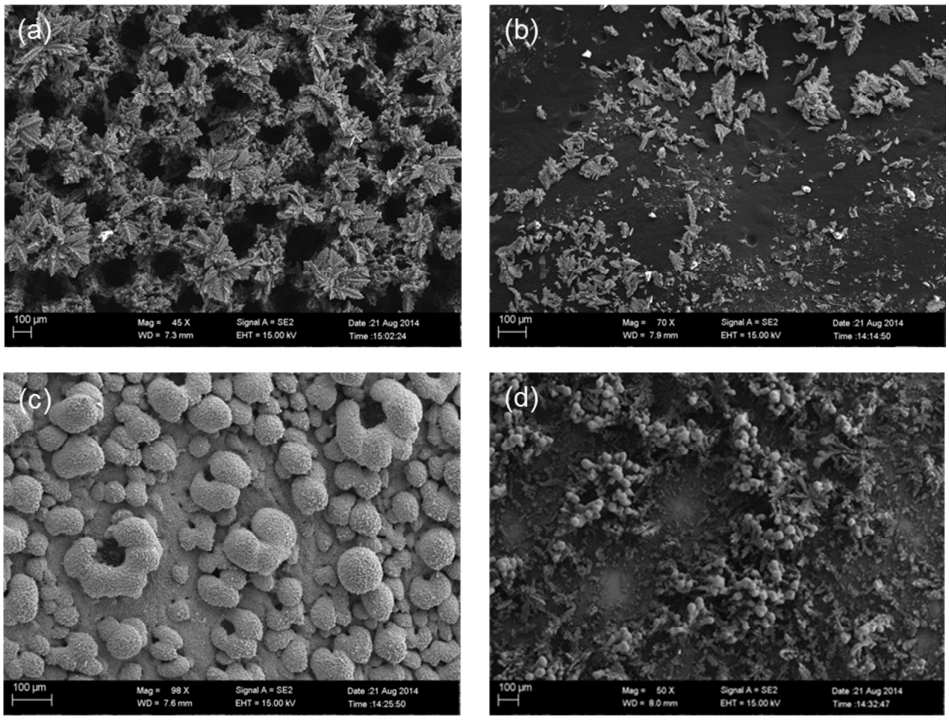

Fig. 7

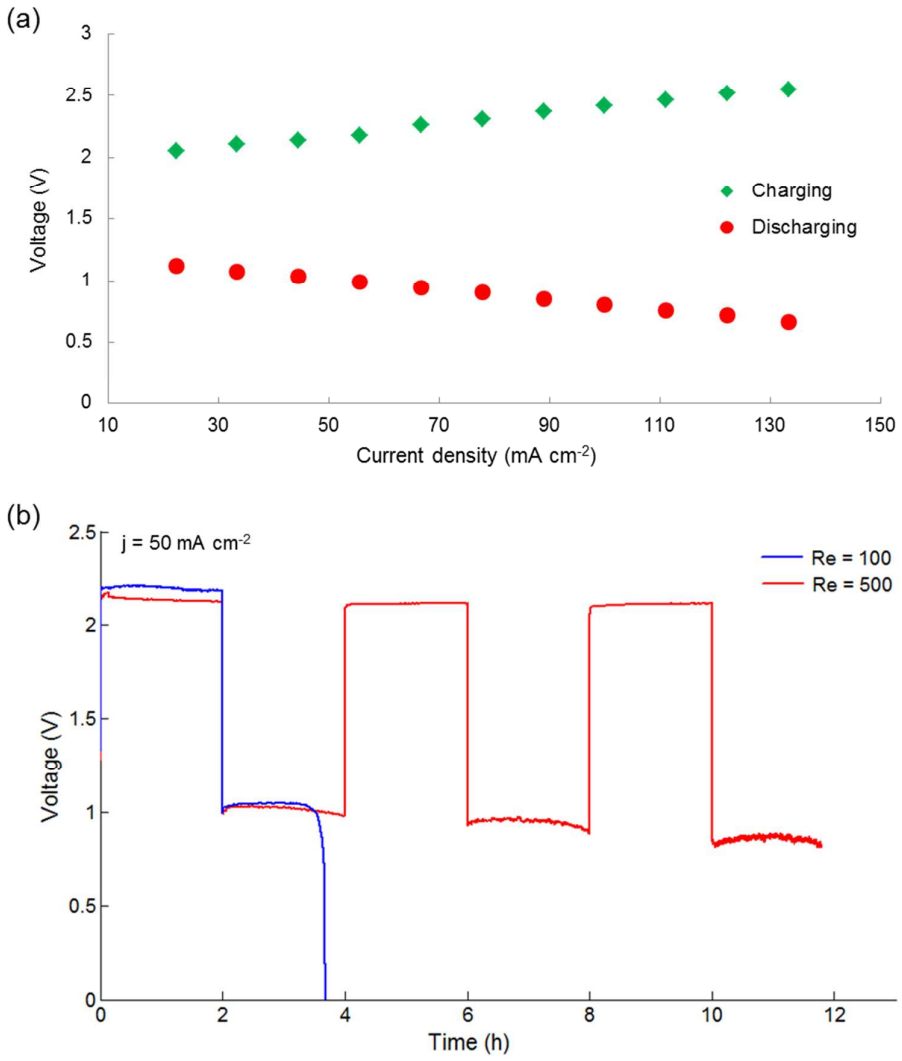

Fig. 8

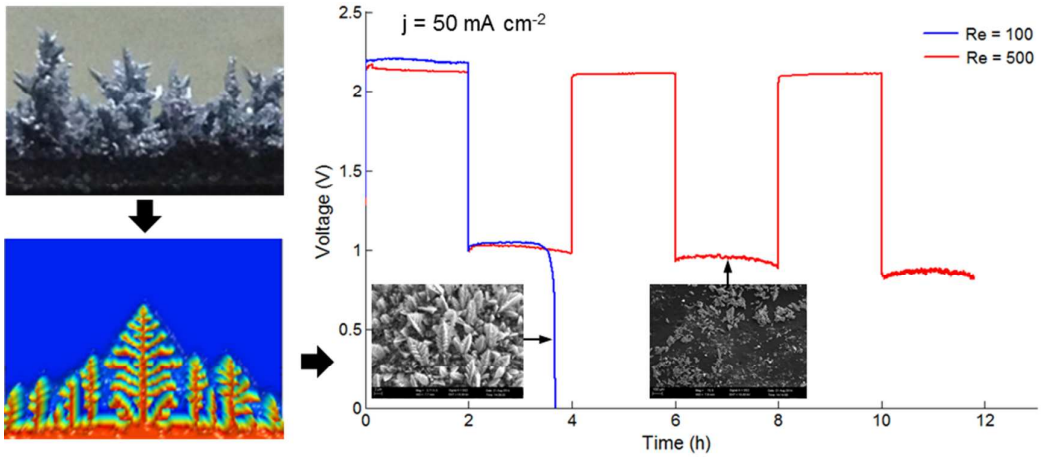

Zinc dendrite growth is controlled by electrolyte flow at high current densities, effectively extending cycle life of rechargeable zinc-air battery.